NEOPLASIA
www.neoplasia.com

Volume 19 Number 12 December 2017 pp. 1022–1032 1022

Cysteine Dioxygenase 1 Mediates Erastin-Induced Ferroptosis in Human Gastric Cancer Cells[1]

Shihui Hao*,[2], Jiang Yu†,[2], Wanming He*, Qiong Huang*, Yang Zhao*, Bishan Liang*, Shuyi Zhang*, Zhaowei Wen*, Shumin Dong*, Jinjun Rao‡, Wangjun Liao* and Min Shi*

*Department of Oncology, Nanfang Hospital, Southern Medical University, Guangzhou, Guangdong 510515, PR China; †Department of General Surgery, Nanfang Hospital, Southern Medical University, Guangzhou, Guangdong 510515, PR China; ‡Key Laboratory of New Drug Screening of Guangdong Province, School of Pharmaceutical Sciences, Southern Medical University, Guangzhou, Guangdong 510515, PR China

Abstract

BACKGROUND: Ferroptosis is a recently discovered form of iron-dependent nonapoptotic cell death. It is characterized by loss of the activity of the lipid repair enzyme, glutathione peroxidase 4 (GPX4), and accumulation of lethal reactive lipid oxygen species. However, we still know relatively little about ferroptosis and its molecular mechanism in gastric cancer (GC) cells. Here, we demonstrate that erastin, a classic inducer of ferroptosis, induces this form of cell death in GC cells and that cysteine dioxygenase 1 (CDO1) plays an important role in this process. *METHODS:* We performed quantitative real-time polymerase chain reaction, Western blotting, cell viability assay, reactive oxygen species (ROS) assay, glutathione assay, lipid peroxidation assay, RNAi and gene transfection, immunofluorescent staining, dual-luciferase reporter assay, transmission electron microscopy, and chromatin immunoprecipitation assay to study the regulation of ferroptosis in GC cells. Mouse xenograft assay was used to figure out the mechanism *in vivo*. *RESULTS:* Silencing CDO1 inhibited erastin-induced ferroptosis in GC cells both *in vitro* and *in vivo*. Suppression of CDO1 restored cellular GSH levels, prevented ROS generation, and reduced malondialdehyde, one of the end products of lipid peroxidation. In addition, silencing COO1 maintained mitochondrial morphologic stability in erastin-treated cells. Mechanistically, c-Myb transcriptionally regulated CDO1, and inhibition of CDO1 expression upregulated GPX4 expression. *CONCLUSIONS:* Our findings give a better understanding of ferroptosis and its molecular mechanism in GC cells, gaining insight into ferroptosis-mediated cancer treatment.

Neoplasia (2017) 19, 1022–1032

Background

Cell death and cell survival are fundamental processes that maintain normal development and homeostasis of organisms [1]. Dysregulation of cell death can result in many pathological phenomena, including infections, neurodegenerative diseases, and cancer [2,3]. Ferroptosis, a novel form of regulated cell death, was identified by Stockwell's group in 2012 [4]. It is an iron-dependent and peroxidation-driven mode of nonapoptotic programmed cell death

Abbreviations: CDO1, cysteine dioxygenase 1; GC, gastric cancer; GPX4, glutathione peroxidase 4; GSH, glutathione; L-ROS, lipid reactive oxygen species; MDA, malondialdehyde; ROS, reactive oxygen species; Xc, glutamate/cystine antiporter

Address all correspondence to: Min Shi, Department of Oncology, Nanfang Hospital, Southern Medical University, Guangzhou, Guangdong 510515, PR China.
E-mail: nfyyshimin@163.com

[1] Funding: This work was supported by the National Natural Science Foundation of China (grant number 81472317), the Science and Technology Planning Project of Guangdong Province (grant number 2016A020215232), the CSCO-Merck Serono Oncology Research Fund (grant number Y-MX2014-048), and the Special Foundation of National Clinical Specialties of China (to the Department of Oncology, Nanfang Hospital).

[2] Contributed equally.

Received 2 August 2017; Revised 20 October 2017; Accepted 23 October 2017

1476-5586
https://doi.org/10.1016/j.neo.2017.10.005

that is characterized by the accumulation of lethal lipid reactive oxygen species (L-ROS) [5,6]. Ferroptosis is distinct from apoptosis, necrosis, and other forms of cell death in terms of its morphology, genetics, metabolism, and molecular biology [4,5]. For example, one essential morphologic feature of ferroptotic cells is smaller mitochondrial sizes and condensed membrane density [4]. The lipid repair enzyme, glutathione peroxidase 4 (GPX4), is increasingly recognized as a negative key regulator of ferroptosis by limiting lipid hydroperoxide levels [7–10]. The existence of ferroptosis has been confirmed in various tumorous cells such as fibrosarcoma [11], lung cancer [12], osteosarcoma [13], kidney cancer [9], and prostate cancer cells [8,14]. Although ferroptosis is implicated in human diseases, its precise regulatory mechanism and biological functions remain elusive.

As a classic inducer of ferroptosis, erastin suppresses the glutamate/cystine antiporter (system X_C^-), thereby inhibiting cellular cystine uptake and depleting glutathione (GSH), a primary cellular antioxidant that maintains the redox balance and defends against oxidative stress [10]. GPX4 uses GSH to repair lipids and reduce lipid hydroperoxides to nontoxic alcohols [9]. A decreased GSH level inactivates GPX4. Subsequently, cells fail to protect against toxic L-ROS, finally incurring ferroptosis.

Human cysteine dioxygenase 1 (CDO1), a non–heme iron metalloenzyme, transforms cysteine to taurine by catalyzing the oxidation of cysteine to its sulfinic acid [15,16]. Increasing CDO1 activity can prevent cytotoxicity from elevated cysteine levels. However, in addition to transforming into taurine, cellular cysteine is also an indispensable substrate for the synthesis of GSH, which consists of glutamate, cysteine, and glycine [17]. A deficiency of cellular cysteine decreases GSH synthesis and impairs cellular antioxidant capacity, which ultimately results in enhanced ROS levels and the induction of ferroptosis [9,18,19]. Therefore, it is reasonable to speculate that CDO1 competitively limits the availability of cysteine to synthesize GSH and influences the process of ferroptosis.

In this study, we demonstrate that erastin induces ferroptosis in gastric cancer (GC) cells and identified the potential relevance of CDO1 in this process. We describe a novel role of CDO1 in regulating erastin-induced ferroptosis, which forecasts a promising future in ferroptosis-mediated tumor therapy.

Methods

Cell Culture and Cell Lines

The AGS, BGC823, MKN45, SGC7901, and MGC803 human GC cell lines were obtained from KeyGEN BioTECH (Nanjing, China). Cells were cultured in RPMI 1640 medium with 10% fetal bovine serum (Thermo Scientific, USA) at 37°C under 5% CO_2.

Tissues

Tumor samples were obtained from 16 patients undergoing surgical resection with curative intent between January and July 2016 in Nanfang Hospital (China).

Reagents and Antibodies

Erastin (#S7242), ferrostatin-1 (#S7243), liproxstatin-1 (#S7699), Z-VAD-FMK (#S7023), necrostatin-1 (#S8037), and 3-methyladenine (#S2767) were obtained from Selleck Chemicals (Houston, TX). Antibodies to CDO1 (#ab53436), GPX4 (#ab125066), and prostaglandin-endoperoxide synthase 2 (PTGS2) (#ab179800) were obtained from Abcam (Cambridge, UK). The antibody to C-Myb (#A3282) was obtained from ABclonal (Woburn, MA). The antibody to glyceraldehyde 3-phosphate dehydrogenase (GAPDH) (#KC5G5) was obtained from KangChen Bio-tech (Shanghai, China). Horseradish peroxidase–conjugated goat anti-rabbit IgG (#4050-05) was from Southern Biotech (Birmingham, AL).

Western Blotting

Protein extracts were separated by using 12% sodium dodecyl sulfate polyacrylamide gels. After electrophoresis, proteins were transferred onto a polyvinylidene membrane and blocked with 5% skim milk in TBST for 1 hour. The primary antibodies were applied overnight at 4°C, and the secondary antibody treatment was applied for about 1 hour at room temperature. The immunoblots were assessed by an Odyssey infrared laser image analysis system (Li-COR Biosciences, Lincoln, NE).

Quantitative Real-Time Polymerase Chain Reaction (qRT-PCR)

Total RNA was extracted from cultured cells using a Trizol kit according to the manufacturer's instructions and then reverse transcribed using the Takara RT reagent (Takara Bio, Shiga, Japan). The primer sequences used for qRT-PCR are listed in Table 1. Expression of candidate genes was normalized to that of GAPDH/β-actin. qRT-PCR was performed using a LightCycler 480 system version 1.5 (Roche, Penzberg, Germany). Samples were run and analyzed in triplicate.

Cell Viability Assay

Cells were cultured in 96-well plates and exposed to various concentrations of the cytotoxic compounds for the indicated times. Thiazolyl blue (3-(4,5-dimethyl-2-thiazolyl)-2,5-diphenyl-2H-tetrazolium bromide, MTT) (5 mg/ml) was added to each well and incubated at 37°C in 5% CO_2 for 4 to 6 hours. Then, 150 μl of dimethyl sulfoxide was added to each well, and the plate was well oscillated. Absorbance of each well was measured at 570 nm using a SpectraMax M5 microplate reader (Molecular Devices, Sunnyvale, CA). The average percentage of inhibition at each concentration was calculated.

ROS Assay

Cells were seeded at 3×10^5 cells per well in 6-well plates. The next day, cells were transfected with CDO1 small interfering (si)RNA using Lipofectamine 2000 (Invitrogen, Carlsbad, CA) for 4 to 6 hours. After 20 hours, the cells were treated with erastin (10 μg/ml) or dimethyl sulfoxide for 24 hours. Cells were incubated with 2 μl 2′,7′-dichlorofluorescin diacetate for 1 hour at 37°C in the dark to

Table 1. Real-Time Polymerase Chain Reaction Primers

Gene	Sequence (5′-3′)
CDO1-F	TCTCTGTTGGGGTGAAGGAC
CDO1-R	GCCAGGCAAATAATGTCTCC
GPX4-F	ACCGAAGTAAACTACACTCAG
GPX4-R	GGCGAACTCTTTGATCTCTT
c-Myb-F	GAAAGCGTCACTTGGGGAAAA
c-Myb-R	TGTTCGATTCGGGAGATAATTGG
Slc7a11-F	TCTCCAAAGGAGGTTACCTGC
Slc7a11-R	AGACTCCCCTCAGTAAAGTGAC
β-actin-F	TGGCACCCAGCACAATGAA
β-actin-R	CTAAGTCATAGTCCGCCTAGAAGCA
GAPDH-F	ACCCAGAAGACTGTGGATGG
GAPDH-R	TCTAGACGGCAGGTCAGGTC

assess cytosolic ROS. Samples were then centrifuged at 1000*g* for 3 minutes, and the pellets were resuspended in 500 µl phosphate-buffered saline (PBS). Measurements were performed on a FACSCalibur (BD Biosciences, San Jose, CA) flow cytometer.

GSH and Lipid Peroxidation Assays

The GSH and malondialdehyde (MDA) contents in cell lysates were assessed using GSH (#ab138881) and lipid peroxidation (#ab118970) assay kits, respectively, according the manufacturer's (Abcam) instructions.

LDH Release Assay

LDH release was assessed using a LDH Assay Kit (#ab65393, Abcam) according to the manufacturer's instructions.

siRNA and Gene Transfection

AGS and BGC823 GC cells were seeded into six-well plates. Once the cells reached 90% confluence, they were transfected with targeted or control siRNA using Lipofectamine 2000 as instructed by the manufacturer. The siRNA sequences are listed in Table 2.

Immunofluorescence Staining

Cells were fixed in 4% formaldehyde for 10 minutes and then incubated in 1% bovine serum albumin in 0.1% PBS-Tween for 1 hour to permeabilize the cells and block nonspecific protein-protein interactions. The cells were then incubated with the GPX4 antibody (1:200) overnight at 4°C. The secondary antibody was Alexa Fluor 488 goat anti-rabbit IgG used (1:200) for 1 hour. 4′,6-Diamidino-2-phenylindole (1.43 µM) was used to stain the cell nuclei blue. Cells were washed three times for 5 minutes with PBS, and photos were taken using fluorescence and laser confocal microscopes.

Dual-Luciferase Reporter Assay

To test for promoter activity, the firefly luciferase gene present in the pGL3-CDO1-promoter and a c-Myb overexpression plasmid with the pcDNA3.1(+) or pcDNA3.1(+)-MYB vectors were purchased from OBiO (Shanghai, China). Cells were seeded at 5000 per well in 96-well plates and transfected with plasmids using Lipofectamine 2000 according to manufacturer's instructions. Transfection conditions were: PGL3-CDO1-promoter, Renilla, Lipofectamine 2000 = 0.1 µg, 0.002 µg, and 0.25 µl per well, respectively. pcDNA3.1(+)-MYB (or pcDNA3.1(+)), Lipofectamine 2000 = 0.1 µg and 0.25 µl, respectively, for the same well. The promoter-luciferase constructs were assessed using a dual-luciferase reporter assay system (E1910; Promega, Madison, WI) according to the manufacturer's instructions.

Table 2. siRNA Sequences

Gene	Sequence
CDO1-siRNA (1)	5′GCGAUGAGGUCAAUGUAGA dTdT 3′ 3′dTdT CGCUACUCCAGUUACAUCU 5′
CDO1-siRNA (2)	5′CCAUCAUGGAAGCCUACGA dTdT 3′ 3′dTdT GGUAGUACCUUCGGAUGCU 5′
CDO1-siRNA (3)	5′ACGCCAAGUUCGACCAGUA dTdT 3′ 3′dTdT UGCGGUUCAAGCUGGUCAU 5′
C-Myb-siRNA (1)	5′GGAACAGAAUGGAACAGAU dTdT 3′ 3′dTdT CCUUGUCUUACCUUGUCUA 5′
C-Myb-siRNA (2)	5′GGUUAUCUGCAGGAGUCUU dTdT 3′ 3′dTdT CCAAUAGACGUCCUCAGAA 5′
C-Myb-siRNA (3)	5′GCACUUGCAGCUCAAGAAA dTdT 3′ 3′dTdT CGUGAACGUCGAGUUCUUU 5′

Chromatin Immunoprecipitation (ChIP) Assay

BGC823 cells (1-2 × 10^7) were grown in a 100 mm dish and cross-linked by adding formaldehyde to a final concentration of 1% and incubating at room temperature for 10 minutes. The ChIP assay was performed according to the assay kit protocol (26,156; Thermo Fisher Scientific, Waltham, MA). The primers for the predicted binding site are listed in Table 3.

Mouse Xenograft Assay

To generate murine subcutaneous tumors, 1 × 10^6 BGC823 control or CDO1 short hairpin (sh)RNA treated cells in 150 µl PBS were injected subcutaneously right of the dorsal midline in athymic nude mice. Once the tumors reached 80 to 100 mm^3 at day 10, mice were allocated randomly into groups of five and treated with erastin (30 mg/kg intraperitoneally, twice every other day). Tumors were measured three times weekly, and volumes were calculated using the formula: length × $width^2$ × π/6. Four weeks after beginning treatment, the tumors were removed.

Statistical Analyses

Unless otherwise indicated, data are expressed as means ± SD of three independent experiments. Unpaired Student's *t* tests were used to compare the means of two groups. A one-way analysis of variance was used for comparison among multiple groups. When the result was significant, *post hoc* testing of differences between groups was performed using the least significant difference test. A *P* value less than .05 was considered significant.

Results

Contribution of CDO1 Suppression to Ferroptosis Resistance

To investigate whether erastin induced ferroptosis in GC cells, we first treated GC cells including AGS, BGC823, MKN45, MGC803, and SGC7901 cells with 0, 2.5, 5, 10, 15, 20, and 40 µg/ml erastin for 24 hours. The MTT assay showed that erastin inhibited the growth of GC cells (Figure 1*A*). GPX4 is one of the most important antioxidant enzymes in mammals, which is also a novel negative mediator in ferroptosis [8]. qRT-PCR showed that, compared to MKN45, MGC803, and SGC7901, GPX4 mRNA levels were obviously decreased in AGS and BGC823 GC cells (Figure 1*B*). We chose AGS and BGC23 GC cells for further research. Importantly, erastin-induced cell death was significantly reversed by the ferroptosis inhibitors ferrostain-1 and liprostatin-1, but not apoptosis, necroptosis, or autophagy inhibitors (ZVAD-FMK, necrostatin, and 3-methyladenine, respectively; Figure 1*C*). Lactate dehydrogenase (LDH) is a soluble cytosolic enzyme that is released into the culture medium following the loss of membrane integrity resulting from necrosis [20]. LDH release assay showed that erastin did not significantly elevate the LDH release in GC cells (Figure 1*D*). These results indicate that erastin-induced cell death is indeed ferroptosis.

Table 3. Primers for the Predicted Binding Site

Binding Site	Sequence (5′-3′)
CDO1 promoter 1-F	CAATGCAATATCAGCACACCTC
CDO1 promoter 1-R	GCAAAGGGTCTGTGCCATTTC
CDO1 promoter 2-F	GAGGAGTCAGAGAAAGAAAATG
CDO1 promoter 2-R	CTTCATTTCAGCTAGTCTAATC
CDO1 promoter 3-F	ACCTTTCTTGGGTGGCTCTC
CDO1 promoter 3-R	CACAAATCAGGTTCAGATCTGT

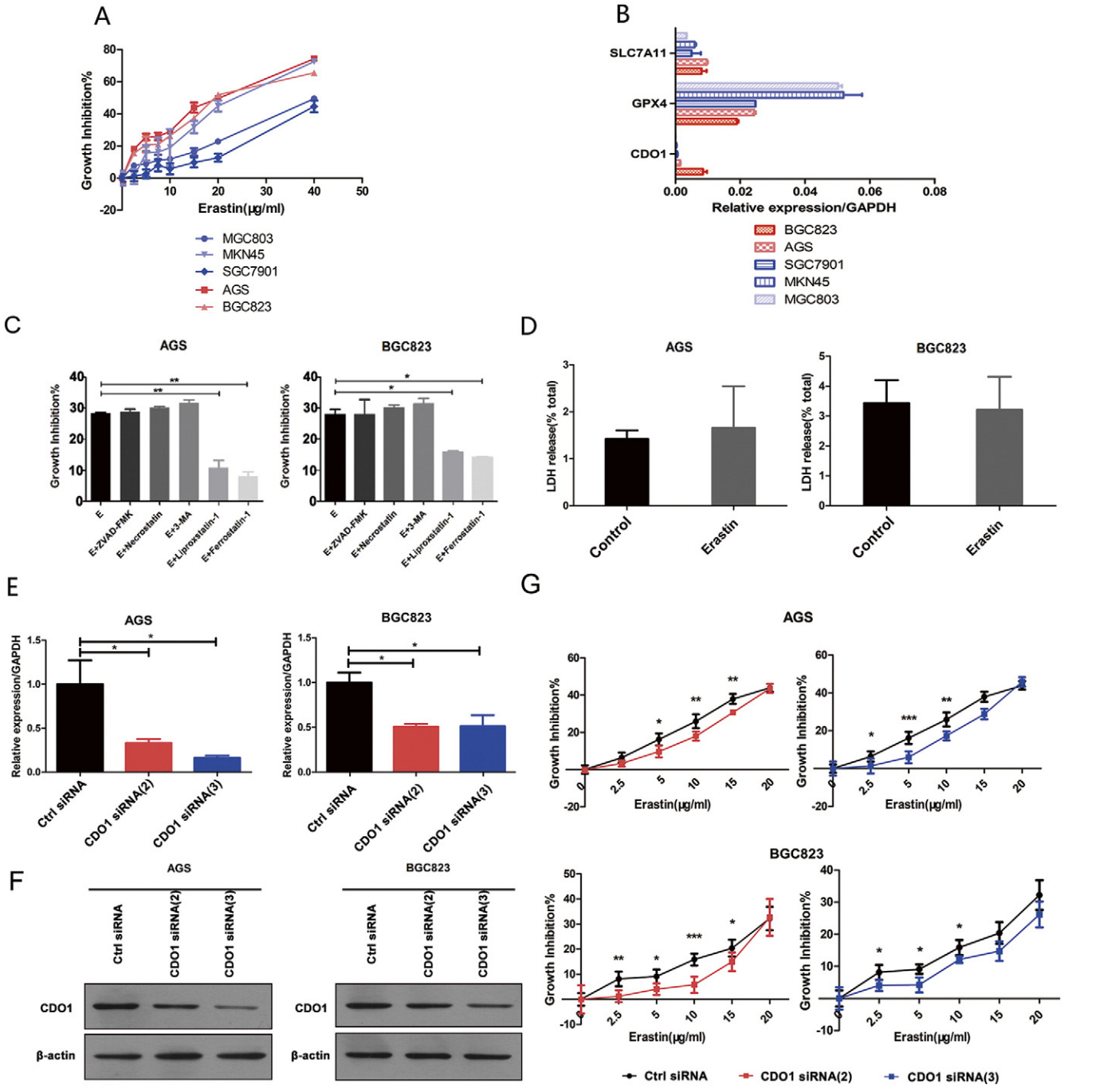

Figure 1. CDO1 suppression contributes to ferroptosis resistance. (A) GC cells were treated with 0, 2.5, 5, 10, 15, 20, or 40 μg/ml erastin for 24 hours. Cell viabilities were assayed by the MTT assay. (B) GPX4, solute carrier family 7 member 11(Slc7a11), and CDO1 expression were assessed by the qRT-PCR in GC cells. (C) GC cells were treated with erastin (E, 10 μg/ml) and with or without Z-VAD-FMK (apoptosis inhibitor), necrostatin (necroptosis inhibitor), 3-methyladenine (3-MA, autophagy inhibitor), and ferrostatin-1 or liproxstatin-1 (ferroptosis inhibitors) for 24 hours. Cell viability was assayed by the MTT assay. (D) GC cells were treated with or without erastin (10 μg/ml). LDH release assay was examined. (E) The siRNA sequences [CDO1 siRNA (2) and (3)] were designed for silencing CDO1. The mRNA levels of CDO1 in GC cells were examined by qRT-PCR. (F) The siRNA sequences [CDO1 siRNA (2) and (3)] were designed for silencing CDO1. The protein levels of CDO1 in GC cells were examined by Western blotting. (G) CDO1 siRNA (2)– and CDO1 siRNA (3)–silenced GC cells were treated with erastin (0, 2.5, 5, 10, 15, and 20 μg/ml) for 24 hours, and cell viabilities were assayed by the MTT assay. Quantitative data are presented as means ± SD from three independent experiments. $P < .05$, $P < .01$, $P < .001$.

Thereafter, we detected the expression of CDO1 mRNA (16 samples) and protein (4 samples) in paired normal and gastric tumor tissue samples (Supplementary Figure 1, *A* and *B*). The results showed that CDO1 expression in tumor samples was low relative to normal tissue.

To gain insight into the role of CDO1 in ferroptosis, three different specific siRNA sequences [CDO1 siRNA (1), CDO1 siRNA (2), and CDO1 siRNA (3)] were transfected into GC cells. The silencing efficiency of the three sequences was shown by qRT-PCR (Figure 1*E*)

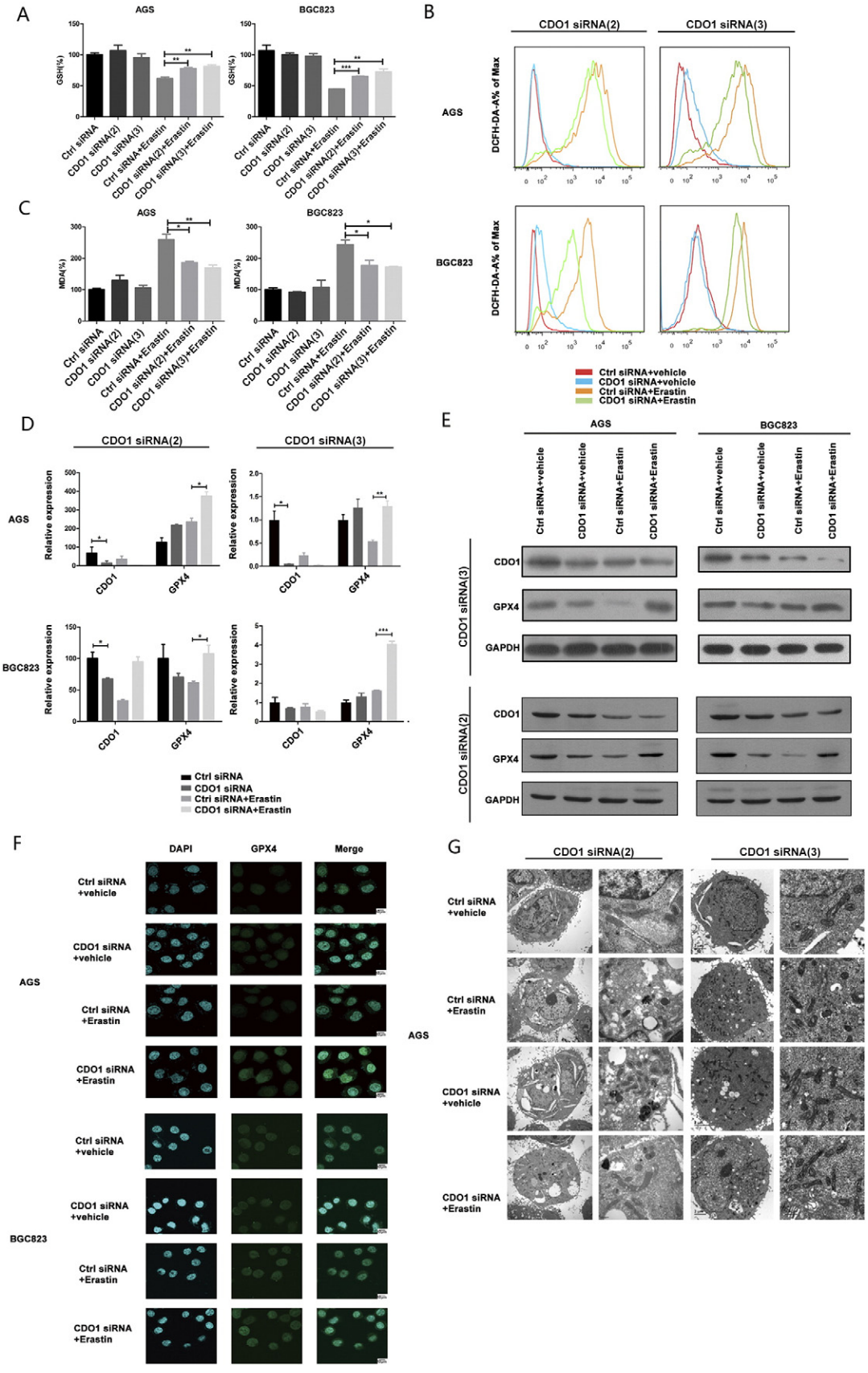

Figure 2. CDO1 regulates ferroptosis biomarkers. CDO1-silenced GC cells were treated with 10 μg/ml erastin for 24 hours. (A) GSH, (B) ROS, and (C) MDA levels were assayed. CDO1 siRNA-silenced GC cells were treated with 10 μg/ml erastin for 24 hours. GPX4 expression was assessed by the qRT-PCR (D), Western blotting (E), and immunofluorescence (F). (G) Transmission electron microscopic images of CDO1 siRNA (2)– and CDO1 siRNA(3)–silenced AGS cells treated with 10 μg/ml erastin for 24 hours. Left, 1×10^4 magnification, scale bar = 2 μm; right, 5×10^4 magnification, scale bar = 500 nm. Quantitative data are presented as means ± SD from three independent experiments. $P < .05$, $P < .01$, $P < .001$.

and Western blotting (Figure 1*F*). We found that CDO1 siRNA (2) and (3) decreased CDO1 mRNA and protein levels. The cell viability analysis [20–22] showed that erastin-induced ferroptosis was inhibited in CDO1-slienced GC cells (Figure 1*G*). In contrast, overexpression of CDO1 promoted erastin-induced ferroptosis (Supplementary Figure 1*C*). Based on these findings, we suggest that erastin can induce ferroptosis in GC cells and CDO1 suppression contributes to ferroptosis resistance.

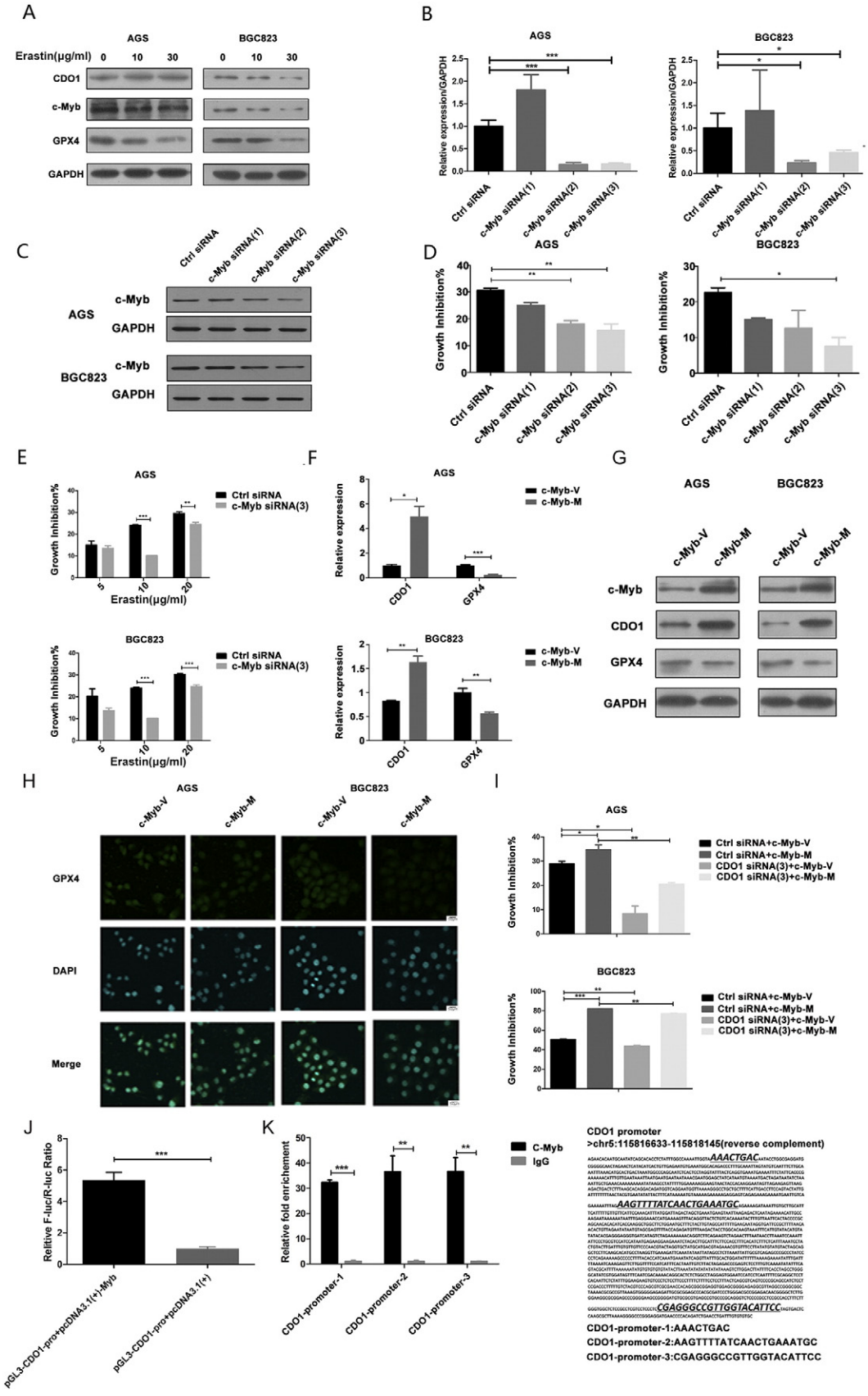

Regulation of CDO1 on Ferroptosis Biomarkers

Previous studies demonstrated that erastin targets system X_C^- and inhibits cystine uptake, subsequently leading to increased ferroptotic events including GSH depletion, GPX4 inactivation, ROS increases, and changes in mitochondrial morphology [9,10,12,23]. To further explore the regulatory role of CDO1 in ferroptosis, we measured the levels of GSH, a key regulator that maintains cellular redox homeostasis [21,24], after suppressing CDO1 expression in erastin-treated GC cells. GSH levels were restored when CDO1 was silenced with CDO1-siRNA during erastin-induced ferroptosis (Figure 2*A*). Moreover, basal ROS levels in CDO1-silenced GC cells with CDO1-siRNA(2) and CDO1-siRNA(3) were maintained with erastin treatment when compared to the control group (Figure 2*B*). MDA, one of the end products of lipid peroxidation [21,24–26], as expected, was greatly decreased when CDO1 expression was suppressed during erastin-induced ferroptosis (Figure 2*C*).

It is well acknowledged that GPX4 is an essential negative regulator and the most important GSH-dependent enzyme in the ferroptosis process [9]. Hence, we sought to investigate the relationship between CDO1 and GPX4. qRT-PCR and Western blotting showed that, compared to the control group, GPX4 mRNA and protein expression was obviously enhanced when CDO1 was suppressed in erastin-induced ferroptosis (Figure 2, *D* and *E*). Similar results were obtained with immunofluorescence staining of GPX4 (Figure 2*F*). In contrast, overexpression of CDO1 repressed GPX4 expression in erastin-treated GC cells (Supplementary Figure 2). These results indicate that CDO1 restrains the inhibitory role of GPX4 in erastin-induced ferroptosis.

We assessed the mitochondrial morphology of GC cells in ferroptosis by transmission electron microscopy. Erastin-treated GC cells contained smaller mitochondria and increased membrane density, consistent with previous studies [4,27,28]. This mitochondrial feature was prevented in CDO1-silenced GC cells treated with erastin (Figure 2*G*). Collectively, these findings suggest that suppression of CDO1 restores cellular GSH levels and prevents increases in cellular ROS, which contributes to resistance from erastin-induced ferroptosis.

C-Myb Regulating CDO1 Expression during Ferroptosis

C-Myb, a proto-oncogene protein, is a transcription factor playing a crucial role in the regulation of hematopoiesis [29,30]. Previous studies demonstrated that benzene toxicity is regulated through the c-Myb signaling pathway and involves alterations in ROS [31]. Furthermore, the CDO1 promoter contains a c-Myb–responsive element (gttg) at −71, and upregulation of c-Myb may boost CDO1 expression [32,33]. Given the interaction of c-Myb with ROS and CDO1, we hypothesized that c-Myb mediated CDO1 expression in erastin-induced ferroptosis.

To verify our hypothesis, we first treated GC cells with 10 or 30 μg/ml erastin for 24 hours. Western blotting showed that c-Myb, CDO1, and GPX4 protein expression levels were decreased under erastin treatment (Figure 3*A*). Next, three diverse siRNAs [c-Myb siRNA (1), (2), and (3)] were used to silence c-Myb. qRT-PCR (Figure 3*B*) and Western blotting (Figure 3*C*) showed that c-Myb mRNA and protein expression levels were decreased with c-Myb siRNA (2) and c-Myb siRNA (3). Growth inhibition with c-Myb siRNA (3) was greatest (Figure 3*D*). Thus, c-Myb siRNA (3) was used to conduct further experiments. Figure 3*E* shows that erastin-induced ferroptosis was restrained when c-Myb was suppressed.

According to the transcription factor binding profile JASPAR CORE and PROMO databases, c-Myb contains a DNA binding domain that is important for its interaction with CDO1. To test this finding, we analyzed mRNA and protein expression levels of CDO1 and GPX4 in GC cells overexpressing c-Myb. The results showed that GPX4 expression was dramatically decreased, while CDO1 was significantly upregulated, in response to the overexpression of c-Myb (Figure 3, *F* and *G*). Similar results were obtained with immunofluorescence staining for GPX4 (Figure 3*H*).

To further investigate whether the role of CDO1 in ferroptosis was regulated transcriptionally by c-Myb, growth inhibition was detected by the MTT assay after overexpression of c-Myb as well as underexpression of CDO1. Silencing CDO1 decreased the promoting effect of c-Myb on erastin-induced ferroptosis (Figure 3*I*). The luciferase reporter assay further demonstrated the direct interaction between c-Myb and CDO1 response elements (Figure 3*J*). Moreover, the ChIP assay showed that c-Myb had three positive binding sites with the CDO1 promoter (Figure 3*K*). Together, these results suggest that c-Myb interacts with the CDO1 promoter as a transcription factor and regulates CDO1 expression and GPX4 during the process of ferroptosis in GC cells.

Suppression of CDO1 Inhibiting Ferroptosis In Vivo

To evaluate the effect of CDO1 on erastin-induced ferroptosis *in vivo*, GC cells with stably inhibited CDO1 were implanted into the subcutaneous space of the right flank of mice. At day 10, the mice were treated with or without erastin (20 mg/kg intraperitoneally, twice every other day) for 4 weeks. Compared with the control group, erastin treatment reduced the size of tumors formed by BGC823 cells significantly. With the same dose of erastin, tumor sizes grew faster in CDO1 knockdown mice compared with the scrambled control group (Figure 4*A*).

Tumors (Figure 4*B*) and lungs, livers, spleens, kidneys, and hearts (Figure 4*C*) of xenograft nude mice were removed and stained with hematoxylin-eosin. Structures and functions were not significantly different between groups treated with or without erastin (Figure 4*C*).

Figure 3. C-Myb regulates CDO1 expression during ferroptosis. (A) GC cells were treated with erastin (10 or 30 μg/ml) for 24 hours. Expression levels of CDO1, c-Myb, and GPX4 proteins were detected by Western blotting. (B) The siRNA sequences [c-Myb siRNA (1), (2), and (3)] were designed for silencing c-Myb. The mRNA levels of c-Myb in GC cells were examined by qRT-PCR. (C) The siRNA sequences [c-Myb siRNA (1), (2), and (3)] were designed for silencing c-Myb. The protein levels of c-Myb in GC cells were examined by Western blotting. (D) Cell viabilities were determined by the MTT assay after transfection with three different c-Myb siRNA sequences to silence c-Myb expression. (E) c-Myb–silenced GC cells were treated with erastin (5, 10, or 20 μg/ml) for 24 hours, and cell viabilities were detected by the MTT assay.C-Myb was overexpressed, and (F) mRNA and (G) protein expression levels of CDO1 and GPX4 were detected by the qRT-PCR and Western blotting, respectively (V, vector; M, overexpression). (H) Immunofluorescence staining of GPX4 was determined when c-Myb was overexpressed. (I) Cell viabilities were determined by the MTT assay after overexpression of c-Myb or inhibited expression of CDO1 in GC cells treated with erastin (10 μg/ml).(J) The interaction between CDO1 and c-Myb was verified by a luciferase reporter assay. (K) The chromatin immunoprecipitation assay shows that c-Myb has three positive binding sites with the CDO1 promoter.Quantitative data are presented as means ± SD from three independent experiments. $P < .05$, $P < .01$, $P < .001$.

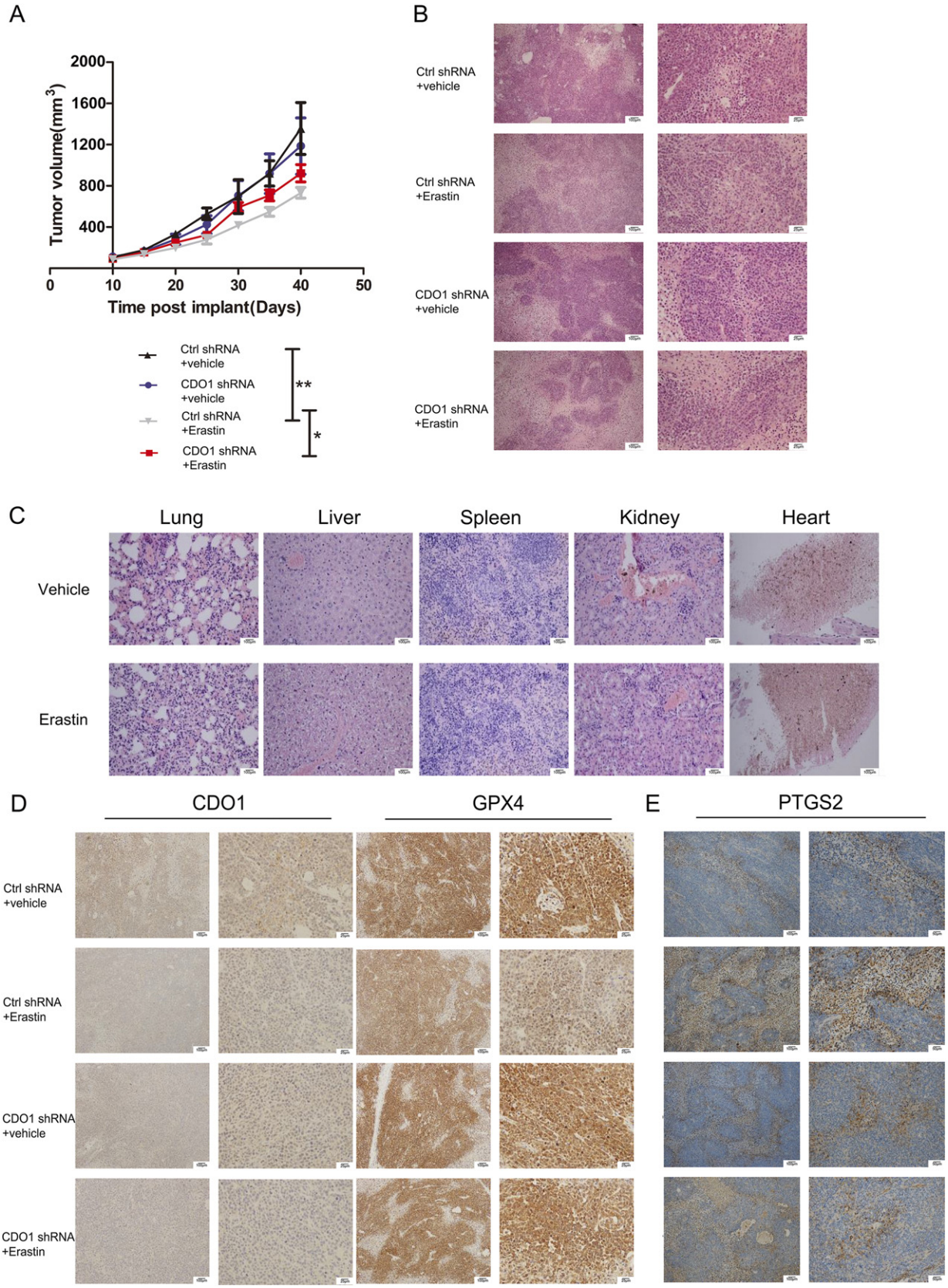

Figure 4. Suppression of CDO1 inhibits ferroptosis *in vivo*. (A) Nude mice were injected subcutaneously with BGC823 cells (1×10^6 cells/mouse) and treated with erastin (20 mg/kg, intraperitoneally, twice every other day) starting at day 10 for 4 weeks. The tumor volume was calculated every 5 days (n = 5). (B, C) Lung, liver, spleen, kidney, heart, and grafted subcutaneous tumors of nude mice were removed and stained with hematoxylin-eosin. Magnification: 100× (left panel), scale bar = 100 μm; 400× (right panel), scale bar = 25 μm. Expression of CDO1, GPX4, and PTGS2 (E) in subcutaneous tumors of nude mice using immunohistochemistry. Magnification: 100× (left panel); scale bar = 100 μm; 200× (right panel), scale bar = 50 μm; 400 × (right panel), scale bar = 25 μm.

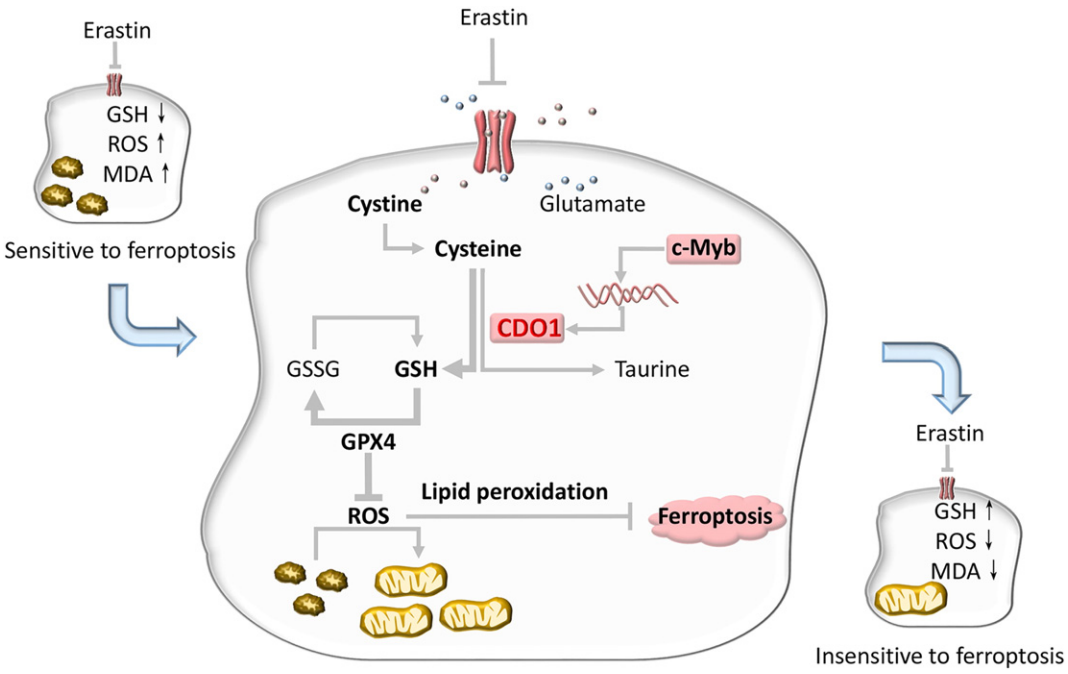

Figure 5. Diagram summarizing the role of CDO1 during erastin-induced ferroptosis.Erastin inhibits cellular cysteine uptake by suppressing system X_C^- and depleting GSH. This leads to inactivation of GPX4, increased ROS, and subsequently ferroptosis. CDO1, transcriptionally regulated by c-Myb, can transform cysteine to taurine and thereby competitively deprive cells of the cysteine used to synthesize GSH. When CDO1 expression is inhibited, the conversion of cysteine to taurine is decreased, enhancing GSH generation. Therefore, GPX4 activity is promoted, inhibiting ROS accumulation and lipid peroxidation and ultimately reducing the risk of ferroptosis.

Immunohistochemical staining of CDO1 and GPX4 showed that GPX4 expression was increased in the shCDO1 group treated with erastin (Figure 4*D*). PTGS2, a marker for the assessment of ferroptosis *in vivo* [9], indicated that genetic inhibition of CDO1 expression renders GC cells less sensitive to erastin (Figure 4*E*). However, immunohistochemical staining of Ki-67 in tumor tissues showed no obvious difference among groups (Supplementary Figure 3).

Discussion

Since the concept of ferroptosis was first reported in 2012, increasing research has revealed that this form of cell death is closely correlated with human diseases. For example, mutated transferrin, an iron exporter, is related to increased neuronal iron accumulation and enhanced susceptibility to Parkinson's disease [34]. Inhibiting ferroptosis by ferrostatin-1 inhibits cell death in cellular models of Huntington's disease, periventricular leukomalacia, and kidney dysfunction [11]. Furthermore, induction of ferroptosis by drugs inhibits cancer cell growth. For example, sorafenib, the first drug used for the systemic treatment of advanced hepatocellular carcinoma, induced ferroptosis in these tumor cells [35]. In addition, artesunate, which recently was shown to induce iron- and ROS-dependent cell death, can suppress the proliferation of both human pancreatic and ovarian cancer cells [36,37]. It was reported that only the AGS GC cell line was sensitive to erastin [4]. However, there was no conclusive evidence for the presence and possible mechanism of ferroptosis in GC cells. In our study, we demonstrate, for the first time, that erastin-induced death of GC cells involves ferroptosis. This information is helpful for an improved understanding of ferroptosis in human malignancies.

Cellular cysteine is mainly obtained from extracellular cystine (the oxidized modality of cysteine) uptake, through system X_C^-. Cystine is then reduced back to cysteine inside the cell [38]. As an essential amino acid, cystine/cysteine is an extracellular nutrient for cancer cells, and its uptake is significant for their viability and growth. System X_C^- was found to be upregulated in many malignant tumors [39] and was associated with chemotherapy resistance [40]. Therefore, deprivation of cysteine may present an attractive therapeutic opportunity.

The system X_C^- inhibitor, sulfasalazine, a medication generally used to treat chronic inflammation, effectively inhibits the growth of lymphoma cells by suppressing system X_C^- [41]. Erastin was identified as a ferroptosis inducer whose mechanism was also to inhibit system X_C^- activity and deprive cells of cysteine [4]. CDO1 can affect cysteine metabolism and determine its flux between GSH and cysteine catabolism/taurine synthesis [42]. Overexpression of CDO1 in breast cancer cells shifted the flux from glutathione synthesis toward cysteine catabolism and increased ROS levels due decreased levels of GSH, leading to reduced cell viability and growth [43]. The results of our study suggest that genetic inhibition of CDO1 expression contributes to the elevated synthesis of GSH as well as deceased ROS levels, ultimately contributing to erastin-induced ferroptosis resistance and then facilitating tumor growth. Our discoveries further support the critical role of cysteine metabolism in ferroptosis and GC cell growth through identifying a new function of CDO1 in ferroptosis.

Apart from being a key enzyme in cysteine biology, CDO1 is also considered to be a tumor suppressor. CDO1 is usually silenced by methylation of its promoter in carcinogenesis. This is associated with distant metastasis and poor prognosis in cancer [43–46]. We found that CDO1 expression in both GC cell lines and tumor samples was relatively low and further discovered that inhibiting CDO1 expression reduced ferroptosis *in vitro* and *in vivo*. From this perspective, our findings imply that the low expression of CDO1 in GC cells may be one

mechanism by which GC cells self-protect themselves from ferroptosis. However, this possibility requires further investigation.

The well-known transcription factor c-Myb has been studied extensively in solid tumors and blood cell malignancies due to its roles in cell proliferation, differentiation, and survival [47]. However, c-Myb is also intimately associated with cellular metabolism. C-Myb is one of the potential DNA elements of the human acyl-CoA synthetase 3 gene, which plays a critical role in fatty acid metabolism [48]. In human dental pulp cells, c-Myb protected against glucose-induced oxidative stress and regulated autophagy [49]. Furthermore, c-Myb influenced taurine accumulation by regulating the taurine transporter [42], and the redox state of cysteine affected the DNA binding activity of c-Myb [50]. Given the important role of cysteine metabolism in erastin-induced ferroptosis, we hypothesized that c-Myb may be involved in the regulation of ferroptosis through CDO1, which can transform cysteine to taurine. We found that expression of both c-Myb and CDO1 was decreased in response to erastin treatment in a dose-dependent manner. We further demonstrated that c-Myb interacted directly with the CDO1 promoter, indicating a role for c-Myb in cysteine metabolism. Additionally, c-Myb can modulate myeloid zinc-finger 1, a transcription factor regulating ferroportin expression, and then regulate iron-related cellular activities and tumor cell growth [51]. However, that study did not demonstrate a relationship between c-Myb and ferroptosis. The current study found that suppression of c-Myb decreased erastin-induced ferroptosis and that overexpression of c-Myb enhanced GPX4 expression. Thus, c-Myb appears to mediate ferroptosis through interaction with CDO1, and cysteine metabolism is probably a key link in this process (See Figure 5).

Overall, the results of the current study provide the first evidence that erastin induces ferroptosis in GC cells and that CDO1 plays a critical role in erastin-induced ferroptosis. Suppression of CDO1 restored GSH levels and GPX4 expression, and diminished ROS levels. We also identified that c-Myb interacted directly with CDO1 and played a significant role in ferroptosis. Future studies on the role of CDO1 in ferroptosis may provide additional novel insights in this field and contribute to developing ferroptosis-mediated therapeutic strategies for human cancer.

Supplementary data to this article can be found online at https://doi.org/10.1016/j.neo.2017.10.005.

Acknowledgements

Not applicable.

References

[1] Vanden Berghe T, Linkermann A, Jouan-Lanhouet S, Walczak H, and Vandenabeele P (2014). Regulated necrosis: the expanding network of non-apoptotic cell death pathways. *Nat Rev Mol Cell Biol* **15**, 135–147.

[2] Kaczmarek A, Vandenabeele P, and Krysko DV (2013). Necroptosis: the release of damage-associated molecular patterns and its physiological relevance. *Immunity* **38**, 209–223.

[3] Suzanne M and Steller H (2013). Shaping organisms with apoptosis. *Cell Death Differ* **20**, 669–675.

[4] Dixon SJ, Lemberg KM, Lamprecht MR, Skouta R, Zaitsev EM, Gleason CE, Patel DN, Bauer AJ, Cantley AM, and Yang WS, et al (2012). Ferroptosis: an iron-dependent form of nonapoptotic cell death. *Cell* **149**, 1060–1072.

[5] Yang WS and Stockwell BR (2016). Ferroptosis: death by lipid peroxidation. *Trends Cell Biol* **26**, 165–176.

[6] Zhao Y, Hu X, Liu Y, Dong S, Wen Z, He W, Zhang S, Huang Q, and Shi M (2017). ROS signaling under metabolic stress: cross-talk between AMPK and AKT pathway. *Mol Cancer* **16**.

[7] Conrad M and Friedmann Angeli JP (2015). Glutathione peroxidase 4 (Gpx4) and ferroptosis: what's so special about it? *Mol Cell Oncol* **2**, e995047.

[8] Friedmann Angeli JP, Schneider M, Proneth B, Tyurina YY, Tyurin VA, Hammond VJ, Herbach N, Aichler M, Walch A, and Eggenhofer E, et al (2014). Inactivation of the ferroptosis regulator Gpx4 triggers acute renal failure in mice. *Nat Cell Biol* **16**, 1180–1191.

[9] Yang WS, SriRamaratnam R, Welsch ME, Shimada K, Skouta R, Viswanathan VS, Cheah JH, Clemons PA, Shamji AF, and Clish CB, et al (2014). Regulation of ferroptotic cancer cell death by GPX4. *Cell* **156**, 317–331.

[10] Xie Y, Hou W, Song X, Yu Y, Huang J, Sun X, Kang R, and Tang D (2016). Ferroptosis: process and function. *Cell Death Differ* **23**, 369–379.

[11] Skouta R, Dixon SJ, Wang J, Dunn DE, Orman M, Shimada K, Rosenberg PA, Lo DC, Weinberg JM, and Linkermann A, et al (2014). Ferrostatins inhibit oxidative lipid damage and cell death in diverse disease models. *J Am Chem Soc* **136**, 4551–4556.

[12] Cao JY and Dixon SJ (2016). Mechanisms of ferroptosis. *Cell Mol Life Sci* **73**, 2195–2209.

[13] Jurkowska H, Stipanuk MH, Hirschberger LL, and Roman HB (2015). Propargylglycine inhibits hypotaurine/taurine synthesis and elevates cystathionine and homocysteine concentrations in primary mouse hepatocytes. *Amino Acids* **47**, 1215–1223.

[14] Gao M, Monian P, Quadri N, Ramasamy R, and Jiang X (2015). Glutaminolysis and transferrin regulate ferroptosis. *Mol Cell* **59**, 298–308.

[15] Joseph CA and Maroney MJ (2007). Cysteine dioxygenase: structure and mechanism. Cambridge, England: Chemical communications; 2007 3338–3349.

[16] Stipanuk MH, Ueki I, Dominy Jr JE, Simmons CR, and Hirschberger LL (2009). Cysteine dioxygenase: a robust system for regulation of cellular cysteine levels. *Amino Acids* **37**, 55–63.

[17] Lu SC (2009). Regulation of glutathione synthesis. *Mol Aspects Med* **30**, 42–59.

[18] Hayano M, Yang WS, Corn CK, Pagano NC, and Stockwell BR (2016). Loss of cysteinyl-tRNA synthetase (CARS) induces the transsulfuration pathway and inhibits ferroptosis induced by cystine deprivation. *Cell Death Differ* **23**, 270–278.

[19] Yu X and Long YC (2016). Crosstalk between cystine and glutathione is critical for the regulation of amino acid signaling pathways and ferroptosis. *Sci Rep* **6**, 30033.

[20] Sun X, Ou Z, Xie M, Kang R, Fan Y, Niu X, Wang H, Cao L, and Tang D (2015). HSPB1 as a novel regulator of ferroptotic cancer cell death. *Oncogene* **34**, 5617–5625.

[21] Sun X, Ou Z, Chen R, Niu X, Chen D, Kang R, and Tang D (2016). Activation of the p62-Keap1-NRF2 pathway protects against ferroptosis in hepatocellular carcinoma cells. *Hepatology* **63**, 173–184.

[22] Kwon MY, Park E, Lee SJ, and Chung SW (2015). Heme oxygenase-1 accelerates erastin-induced ferroptotic cell death. *Oncotarget* **6**, 24393–24403.

[23] Gao M, Monian P, and Jiang X (2015). Metabolism and iron signaling in ferroptotic cell death. *Oncotarget* **6**, 35145–35146.

[24] Yuan H, Li X, Zhang X, Kang R, and Tang D (2016). CISD1 inhibits ferroptosis by protection against mitochondrial lipid peroxidation. *Biochem Biophys Res Commun* **478**, 838–844.

[25] Tsikas D (2017). Assessment of lipid peroxidation by measuring malondialdehyde (MDA) and relatives in biological samples: analytical and biological challenges. *Anal Biochem* **524**, 13–30.

[26] Yahya MD, Pinnas JL, Meinke GC, and Lung CC (1996). Antibodies against malondialdehyde (MDA) in MRL/lpr/lpr mice: evidence for an autoimmune mechanism involving lipid peroxidation. *J Autoimmun* **9**, 3–9.

[27] Dolma S, Lessnick SL, Hahn WC, and Stockwell BR (2003). Identification of genotype-selective antitumor agents using synthetic lethal chemical screening in engineered human tumor cells. *Cancer Cell* **3**, 285–296.

[28] Yagoda N, von Rechenberg M, Zaganjor E, Bauer AJ, Yang WS, Fridman DJ, Wolpaw AJ, Smukste I, Peltier JM, and Boniface JJ, et al (2007). RAS-RAF-MEK-dependent oxidative cell death involving voltage-dependent anion channels. *Nature* **447**, 864–868.

[29] Vargova K, Curik N, Burda P, Basova P, Kulvait V, Pospisil V, Savvulidi F, Kokavec J, Necas E, and Berkova A, et al (2011). MYB transcriptionally regulates the miR-155 host gene in chronic lymphocytic leukemia. *Blood* **117**, 3816–3825.

[30] Baer MR, Augustinos P, and Kinniburgh AJ (1992). Defective c-myc and c-myb RNA turnover in acute myeloid leukemia cells. *Blood* **79**, 1319–1326.

[31] Wan J and Winn LM (2007). Benzene's metabolites alter c-MYB activity via reactive oxygen species in HD3 cells. *Toxicol Appl Pharmacol* **222**, 180–189.

[32] Booken N, Gratchev A, Utikal J, Weiss C, Yu X, Qadoumi M, Schmuth M, Sepp N, Nashan D, and Rass K, et al (2008). Sezary syndrome is a unique cutaneous T-cell lymphoma as identified by an expanded gene signature including diagnostic marker molecules CDO1 and DNM3. *Leukemia* **22**, 393–399.

[33] Ramsden DB, Kapadi A, Fitch NJ, Farmer MJ, Bennett P, and Williams AC (1997). Human cysteine dioxygenase type I (CDO-I; EC 1.13.11.20): 5′ flanking region and intron-exon structure of the gene. *Mol Pathol* **50**, 269–271.

[34] Rhodes SL, Buchanan DD, Ahmed I, Taylor KD, Loriot MA, Sinsheimer JS, Bronstein JM, Elbaz A, Mellick GD, and Rotter JI, et al (2014). Pooled analysis of iron-related genes in Parkinson's disease: association with transferrin. *Neurobiol Dis* **62**, 172–178.

[35] Louandre C, Marcq I, Bouhlal H, Lachaier E, Godin C, Saidak Z, Francois C, Chatelain D, Debuysscher V, and Barbare JC, et al (2015). The retinoblastoma (Rb) protein regulates ferroptosis induced by sorafenib in human hepatocellular carcinoma cells. *Cancer Lett* **356**, 971–977.

[36] Eling N, Reuter L, Hazin J, Hamacher-Brady A, and Brady NR (2015). Identification of artesunate as a specific activator of ferroptosis in pancreatic cancer cells. *Oncoscience* **2**, 517–532.

[37] Greenshields AL, Shepherd TG, and Hoskin DW (2017). Contribution of reactive oxygen species to ovarian cancer cell growth arrest and killing by the anti-malarial drug artesunate. *Mol Carcinog* **56**, 75–93.

[38] McBean GJ (2002). Cerebral cystine uptake: a tale of two transporters. *Trends Pharmacol Sci* **23**, 299–302.

[39] Polewski MD, Reveron-Thornton RF, Cherryholmes GA, Marinov GK, Cassady K, and Aboody KS (2016). Increased expression of system xc- in glioblastoma confers an altered metabolic state and temozolomide resistance. *Mol Cancer Res* **14**, 1229–1242.

[40] Lo M, Ling V, Wang YZ, and Gout PW (2008). The xc- cystine/glutamate antiporter: a mediator of pancreatic cancer growth with a role in drug resistance. *Br J Cancer* **99**, 464–472.

[41] Gout PW, Simms CR, and Robertson MC (2003). In vitro studies on the lymphoma growth-inhibitory activity of sulfasalazine. *Anticancer Drugs* **14**, 21–29.

[42] Han X, Patters AB, Jones DP, Zelikovic I, and Chesney RW (2006). The taurine transporter: mechanisms of regulation. *Acta Physiol (Oxf)* **187**, 61–73.

[43] Jeschke J, O'Hagan HM, Zhang W, Vatapalli R, Calmon MF, Danilova L, Nelkenbrecher C, Van Neste L, Bijsmans IT, and Van Engeland M, et al (2013). Frequent inactivation of cysteine dioxygenase type 1 contributes to survival of breast cancer cells and resistance to anthracyclines. *Clin Cancer Res* **19**, 3201–3211.

[44] Brait M, Ling S, Nagpal JK, Chang X, Park HL, Lee J, Okamura J, Yamashita K, Sidransky D, and Kim MS (2012). Cysteine dioxygenase 1 is a tumor suppressor gene silenced by promoter methylation in multiple human cancers. *PLoS One* **7**, e44951.

[45] Kwon J, Park M, Kim JH, Lee HW, Kang MC, and Park JH (2015). Epigenetic regulation of the novel tumor suppressor cysteine dioxygenase 1 in esophageal squamous cell carcinoma. *Tumour Biol* **36**, 7449–7456.

[46] Ushiku H, Yamashita K, Katoh H, Ema A, Minatani N, Kikuchi M, Kojo K, Yokoi K, Tanaka T, and Nishizawa N, et al (2017). Promoter DNA methylation of CDO1 gene and its clinical significance in esophageal squamous cell carcinoma. *Dis Esophagus* **30**, 1–9.

[47] Nakano K, Uchimaru K, Utsunomiya A, Yamaguchi K, and Watanabe T (2016). Dysregulation of c-Myb pathway by aberrant expression of proto-oncogene MYB provides the basis for malignancy in adult T-cell leukemia/lymphoma cells. *Clin Cancer Res* **22**, 5915–5928.

[48] Minekura H, Kang MJ, Inagaki Y, Suzuki H, Sato H, Fujino T, and Yamamoto TT (2001). Genomic organization and transcription units of the human acyl-CoA synthetase 3 gene. *Gene* **278**, 185–192.

[49] Lee YH, Kim HS, Kim JS, Yu MK, Cho SD, Jeon JG, and Yi HK (2016). C-myb regulates autophagy for pulp vitality in glucose oxidative stress. *J Dent Res* **95**, 430–438.

[50] Guehmann S, Vorbrueggen G, Kalkbrenner F, and Moelling K (1992). Reduction of a conserved Cys is essential for Myb DNA-binding. *Nucleic Acids Res* **20**, 2279–2286.

[51] Chen Y, Zhang Z, Yang K, Du J, Xu Y, and Liu S (2015). Myeloid zinc-finger 1 (MZF-1) suppresses prostate tumor growth through enforcing ferroportin-conducted iron egress. *Oncogene* **34**, 3839–3847.